A Stress-dependent Magnetostriction Model of Amorphous Alloy Based on Microscopic Statistical Constructive Model and Jiles-Atherton Model

Tong Ben1, Xin Qi1, Long Chen1,2*, and Ni An1

¹College of Electrical Engineering and New Energy, China Three Gorges University, Yichang, Hubei 443002, China
²Hubei Provincial Engineering Technology Research Center for Power Transmission Line,
China Three Gorges University, Yichang 443002, China

(Received 10 January 2025, Received in final form 10 June 2025, Accepted 10 June 2025)

This study presents a stress-dependent magnetostriction model that incorporates hysteresis effects to simulate the magnetostriction properties of amorphous alloys in response to variations in magnetic fields and stress. The model is grounded in a microscopic statistical constructive framework. Given the absence of a crystalline structure in amorphous materials, a probability distribution function is developed to account for stress effects, which characterizes the randomly distributed magnetic moments within the amorphous matrix through the concept of locally ordered magnetic moment regions. The relationship between magnetostriction and magnetization is established by integrating the derived stress-dependent magnetostriction expression with a modified anhysteretic magnetization model. Hysteresis effects are addressed by incorporating an irreversible magnetization component, as informed by the inverse Jiles-Atherton theory. The parameters of the model are calibrated using experimental data. The simulation outcomes demonstrate that the proposed model successfully replicates the magnetostriction loop while accounting for stress influences.

Keywords: amorphous alloy, magnetostriction model, microscopic statistical constructive model, inverse JA model

1. Introduction

In contrast to silicon steel materials, amorphous alloys lack a defined crystalline structure and structural imperfections that hinder the movement of magnetic domain walls at the microscopic level. At a macroscopic scale, amorphous alloys exhibit several advantageous properties, including low energy loss, high permeability, and elevated saturation flux density. Specifically, at equivalent frequencies and flux densities, the core loss of amorphous stator materials is approximately 18.4% that of silicon steel stator cores, while their permeability is roughly double that of silicon steel [1]. Consequently, the utilization of amorphous alloys in place of traditional silicon steel for the cores of low-power, high-frequency electrical equipment can lead to a significant reduction in core losses, presenting promising prospects for applications in motor design. However, the thickness of amorphous alloy strips is only one-tenth that of silicon steel, resulting in heightened sensitivity to stress, and their magnetostriction is considerably greater than that of silicon steel, which induces stronger vibrations [2, 3]. If core vibrations are mitigated through the application of stress, the magnetic properties of the core may be compromised. Therefore, it is essential to investigate the mechanisms by which stress influences the magnetization and magnetostriction characteristics of amorphous alloys.

Presently, conventional models of stress-dependent magnetostriction can be developed utilizing various theoretical frameworks, including phenomenological theory, thermodynamic models, magnetic domain theory, and multiscale models. The phenomenological model primarily captures the influence of stress on magnetostriction by incorporating a stress term into the distribution function derived from first-order and second-order slew curves [4]. However, this model is complex, necessitating extensive calculations, and lacks a robust physical interpretation. The thermodynamic model, on the other hand, derives the magnetostriction strain equation through the partial differentiation of Gibbs free energy with respect to stress, offering a more straightforward computational approach. Nonetheless, this model is contingent upon experimental data, and certain parameters are challenging to ascertain [5].

©The Korean Magnetics Society. All rights reserved.

*Corresponding author: Tel: +86-18522089362

e-mail: chenlong@ctgu.edu.cn

The magnetic domain theory model addresses magnetostriction by analyzing domain motion and deflection in relation to domain energy [6], allowing for the consideration of stress effects through the evaluation of magnetoelastic energy. However, this model is characterized by a considerable number of unknown parameters. The multiscale model captures the response of single crystals by examining the behavior of local magnetic fields and stresses at the domain level, subsequently applying the principle of homogenization to extend these insights to polycrystalline materials. Despite its advantages, this model is associated with prolonged computational times and is not suitable for finite element numerical analyses [7]. A simplified multiscale model has been proposed, which assumes that each single crystal comprises six magnetic domains, with the energy of each domain represented by a simplified free energy function, thereby significantly reducing computational time [8]. However, this simplified approach fails to account for the hysteresis effect inherent in magnetostriction. Furthermore, given that amorphous alloys lack a crystalline structure, this model does not adequately address the unique characteristics of amorphous materials. In conclusion, existing magnetostriction models predominantly concentrate on silicon steel materials, neglecting the distinctions present in amorphous alloys. Additionally, some studies yield single-valued curves of magnetostriction in relation to magnetization strength, without adequately considering the hysteresis effect induced by magnetic field excitation and the dependence on stress.

This paper presents an improved magnetostrictive model for amorphous alloys that takes into account the influence of compressive stress. The model effectively correlates macroscopic magnetic behavior with statistical outcomes derived from microscopic behavior, thereby providing a physically coherent framework. The parameters of the model are determined using experimental measurement data, and the validity of the proposed model is substantiated by comparing the simulation results with the relevant experimental findings.

2. Stress-dependent Magnetostriction Model of Amorphous Alloys

2.1. Improved microscopic statistical constructive model

Amorphous alloys do not have a crystal structure and the atomic magnetic moments are usually randomly distributed in an irregular structure resulting in the lack of magnetocrystalline anisotropy properties. Thus, it is regarded as an isotropic material [9]. A schematic illustration of the magnetostriction mechanism in an isotropic material is presented in Fig. 1. Within this diagram, each atom is

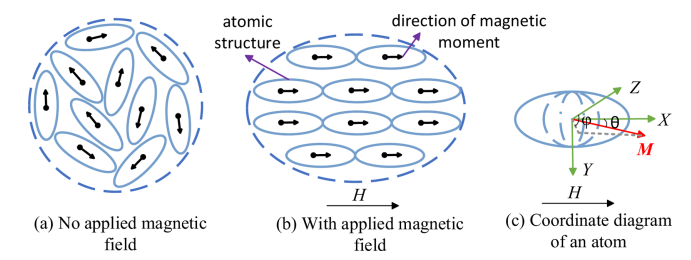


Fig. 1. (Color online) Schematic diagram of magnetostriction mechanism.

individually illustrated by a solid ellipse, and the magnetic moments of the atoms are indicated by arrows. For the macroscopic isotropy of amorphous alloys, the free energy of the atomic magnetic moment can be expressed as the sum of the Seeman energy W_{mag} and the stress anisotropy energy W_{σ} [8]:

$$W_{i} = W_{mag} + W_{\sigma} = -\mu_{0} H M_{s} (\alpha_{1} \gamma_{1} + \alpha_{2} \gamma_{2} + \alpha_{3} \gamma_{3})$$

$$-1.5 \lambda_{100} \sigma (\alpha_{1}^{2} \beta_{1}^{2} + \alpha_{2}^{2} \beta_{2}^{2} + \alpha_{3}^{2} \beta_{3}^{2})$$

$$-3 \lambda_{111} \sigma (\alpha_{1} \alpha_{2} \beta_{1} \beta_{2} + \alpha_{2} \alpha_{3} \beta_{2} \beta_{3} + \alpha_{1} \alpha_{3} \beta_{1} \beta_{3})$$
(1)

where σ represents the applied stress; H and M_s correspond to the external magnetic field and saturation magnetization strength, respectively; the saturation magnetostriction coefficient is given by λ_s ; μ_0 denotes the vacuum permeability; α_m , γ_m and β_m ($m = \{1, 2, 3\}$) are the direction cosines of the magnetization strength M, magnetic field strength H and applied stress σ in the X, Y, Z directions, respectively; λ_{100} , λ_{111} are the magnetostriction coefficients in the [100], [111] directions, respectively.

According to the actual working condition of the stress-actuated amorphous iron core, this paper considers the compressive stress applied perpendicular to the magnetic circuit direction of the core, and the magnetic field direction along the *X*-axis. When the compressive stress is applied along the *Y*-direction, $\beta_1 = \beta_3 = 0$, $\gamma_2 = \gamma_3 = 0$. And since amorphous alloys are macroscopically isotropic, the magnetostriction coefficients of the directions are the same, i.e., $\lambda_{100} = \lambda_{111} = \lambda_s$. The free energy of the magnetic moment then simplifies to:

$$W_{i} = W_{\text{mag}} + W_{\sigma} = -\mu_{0} H M_{s} \alpha_{1} \gamma_{1} - 1.5 \lambda_{s} \sigma \alpha_{2}^{2} \beta_{2}^{2}$$
 (2)

The micro-statistical constructive model is established through probabilistic statistical analysis of the angular dispersion of magnetic moments and the corresponding deformation associated with the orientation of these moments, as shown in Fig. 2; where l_0 represents the length of the initial atomic structure, p_s represents the deformation.

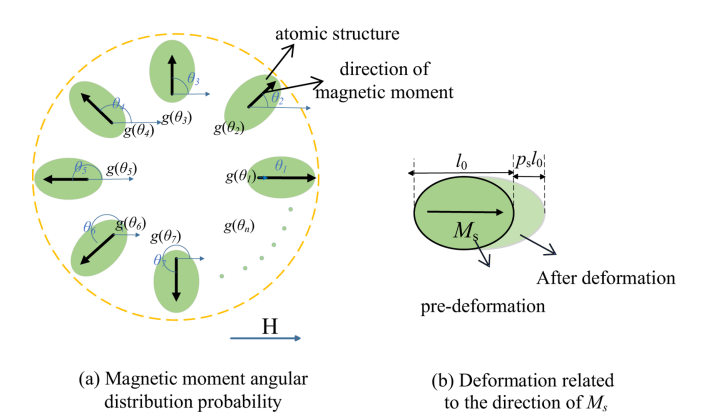


Fig. 2. (Color online) Micro-schematic diagram of the modeling principle.

The modeling approach is to intercept a face of the three-dimensional structure inside the material and divide the magnetic moment distribution on that face into n angles θ [10]. Each atom's magnetic moment i corresponds to a probability distribution $g(\theta_i)$ for that magnetic moment angle. According to the actual working condition of stress action, the compressive stress applied to the core in the direction that is perpendicular to the magnetic circuit is considered in this paper. Therefore, the improved probability distribution function can be expressed as:

$$g_{i}(H,\sigma) = Ue^{-A_{s}W_{i}} = Ue^{\kappa H\cos\theta + \alpha_{s}\sigma\sin^{2}\theta\sin^{2}\varphi}$$
(3)

where U is a normalized function of stress and magnetic field, $\kappa = \mu_0 A_{\rm s} M_{\rm s}$, $\alpha_{\rm s} = 1.5 A_{\rm s} \lambda_{\rm s}$; a material parameter associated with the initial susceptibility χ^0 is represented as $A_{\rm s}$, $A_{\rm s} = 3\chi^0/\mu_0 M_{\rm s}^2$.

The integral of the probability function g to the overall distribution is 1, i.e.:

$$\int g dV = U \int_0^{2\pi} d\varphi \int_0^{\pi} e^{\kappa H \cos\theta + \alpha_s \sigma \sin^2\theta \sin^2\varphi} \sin\theta d\theta = 1$$
 (4)

Once the new probability distribution function is defined, combining Eqs. (3) and (4), the macroscopic magnetization strength M_I of amorphous alloys under applied stress in the Y-direction can be obtained by three-dimensional integration:

$$M_{I} = M_{s} \sum g_{i} \cos \theta_{i}$$

$$= M_{s} \int_{0}^{2\pi} d\varphi \int_{0}^{\pi} \frac{e^{\kappa H \cos \theta + \alpha_{s} \sigma \sin^{2} \theta \sin^{2} \varphi}}{\int_{0}^{2\pi} d\varphi \int_{0}^{\pi} e^{\kappa H \cos \theta + \alpha_{s} \sigma \sin^{2} \theta \sin^{2} \varphi} \sin \theta d\theta} \cos \theta \sin \theta d\theta$$
(5)

2.2. Stress-dependent magnetostriction model of amorphous alloys

Since the micro-statistical model can take into account the effect of stress and the inverse JA model exhibits the hysteresis effect, the two are combined. The anhysteretic magnetization intensity from the inverse JA model is replaced by Eq. (5). And according to the mean-field theory, the magnetic field H in Eq. (5) is corrected to the effective magnetic field H_e [11]. The constructed stress-dependent hysteresis model is represented as:

$$\frac{dM}{dB} = \frac{(1-c)\frac{dM_{irr}}{dB_e} + \frac{cdM_{an}(\sigma, H_e)}{\mu_0 dH_e}}{1 + c(1-\alpha)\frac{dM_{an}(\sigma, H_e)}{dH_e} + \mu_0 (1-c)(1-\alpha)\frac{dM_{irr}}{dB_e}}$$
(6)

where B_e represents the effective magnetic density; α signifies the mean-field coupling inside the magnetic domain; c is the reversible parameter; the stress-related anhysteretic magnetization $M_{an}(\sigma, H_e)$ is expressed as follows:

$$M_{an}(\sigma, H_e) = M_s \int_0^{2\pi} d\varphi \int_0^{\pi} \frac{e^{\kappa H_e \cos\theta + \alpha_s \sigma \sin^2\theta \sin^2\varphi}}{\int_0^{2\pi} d\varphi \int_0^{\pi} e^{\kappa H_e \cos\theta + \alpha_s \sigma \sin^2\theta \sin^2\varphi} \sin\theta d\theta} \cos\theta \sin\theta d\theta$$
(7)

 M_{irr} denotes the irreversible magnetization; dM_{irr}/dB_e is represented as:

$$\frac{\mathrm{d}M_{irr}}{\mathrm{d}B_{e}} = \frac{\delta_{M}(M_{an}(\sigma, H_{e}) - M_{irr})}{\mu_{0}\delta k} \tag{8}$$

Where k represents the pinning parameter; δ_M is the bounding coefficient defined to prevent the emergence of non-physical solutions; δ indicates the direction coefficient.

 $H_{\rm e}$ denotes the effective magnetic field. Since the excitation condition is sinusoidal with an industrial frequency of 50 Hz, a dynamic expansion of the model is required to account for the impacts of both residual loss field $H_{\rm exc}$ and eddy current loss field $H_{\rm eddy}$ on hysteresis [12]. Then the effective magnetic field considering the dynamic field is improved as:

$$H_{e_dyn} = H_e - H_{eddy} - H_{exc}$$

$$= H_e - \frac{vd^2}{12} \frac{dB}{dt} - \delta \sqrt{vSGV_0} \left| \frac{dB}{dt} \right|^{\frac{1}{2}}$$
(9)

where d denotes the thickness of the amorphous alloy, G represents a dimensionless coefficient, G=0.1356, v represents the conductivity of the amorphous alloy material, S signifies the cross-sectional area of the core, and V_0 indicates a statistical parameter of residual loss. Let $k_{eddy} = vd^2/12$, $k_{exc} = (vSGV_0)^{1/2}$, k_{eddy} denotes the eddy current loss coefficient; k_{exc} denotes the residual loss coefficient, obtained by parameter identification of the experimental data in section 3.2.

Thus, the stress-dependent hysteresis model considering

dynamic effects is represented as:

$$\frac{\mathrm{d}M_{dyn}}{\mathrm{d}B} = \frac{(1-c)\frac{\mathrm{d}M_{irr_dyn}}{\mathrm{d}B_e} + \frac{c\mathrm{d}M_{an}(\sigma, H_{e_dyn})}{\mu_0\mathrm{d}H_{e_dyn}}}{1 + c(1-\alpha)\frac{\mathrm{d}M_{an}(\sigma, H_{e_dyn})}{\mathrm{d}H_{e_dyn}} + \mu_0(1-c)(1-\alpha)\frac{\mathrm{d}M_{irr_dyn}}{\mathrm{d}B_e}}$$
(10)

Subsequently, to investigate the magnetostriction properties of amorphous alloys subjected to an external magnetic field and compressive stresses oriented in various directions, the atomic lengths within the cell following deformation along the magnetization axis are derived utilizing an improved probability distribution function:

$$l(H,\sigma) = l_0 + p_s l_0 \sum_{i} g(\theta_i) |\cos \theta_i|$$

$$= l_0 + p_s l_0 \int_0^{2\pi} d\varphi \int_0^{\pi} g(H,\sigma) |\cos \theta| \sin \theta d\theta$$
(11)

Further, the magnetostriction strain based on the deformation associated with the orientation of the magnetic moment is expressed as [10]:

$$\lambda = \frac{l(H,\sigma) - l(H=0,\sigma)}{l_0} = \lambda_0(\sigma = 0)$$

$$+2\lambda_s \left(\int_0^{2\pi} d\varphi \int_0^{\pi} g \left| \cos \theta \right| \sin \theta d\theta - \frac{1}{2} \right)$$

$$= 2\lambda_s \left(\int_0^{2\pi} d\varphi \int_0^{\pi} g(H,\sigma) \left| \cos \theta \right| \sin \theta d\theta - \frac{1}{2} \right)$$
(12)

Where λ_0 denotes the stress-dependent initial magnetostriction. The so-called ΔE effect (change of magnetostriction under stress) proposes an analytical expression for the strain of materials in a state of non-zero stress and zero magnetic field:

$$\lambda_0(\sigma) = \lambda_s \left(1 - \frac{3(e^{\alpha_s \sigma_y} + e^{\alpha_s \sigma_z})}{2(e^{\alpha_s \sigma_x} + e^{\alpha_s \sigma_y} + e^{\alpha_s \sigma_z})}\right) \tag{13}$$

where σ_i is the applied stress along an *i*th direction, $i = \{x, y, z\}$.

In the absence of impediments during the process of magnetization, the work associated with magnetic energy governs the development of the anhysteretic magnetization curve. The conventional representation of the anhysteretic magnetization curve is characterized by a modified Langevin function:

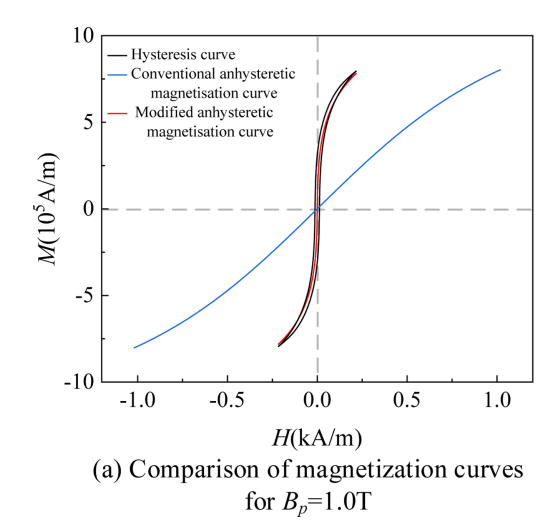
$$M' = M_s \left[\coth\left(\frac{H_e}{a}\right) - \frac{a}{H_e} \right] = M_s \left[\coth\left(\frac{H + \alpha M}{a}\right) - \frac{a}{H + \alpha M} \right]$$
(14)

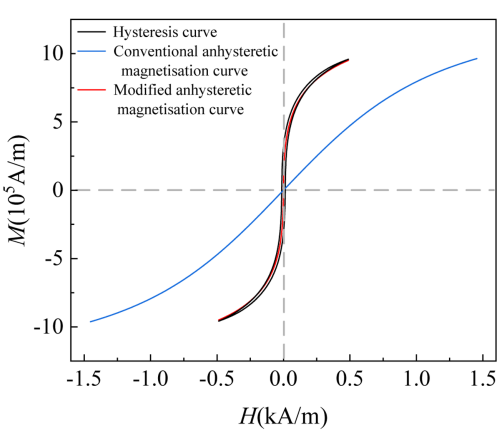
where a signifies the shape parameter of the anhysteretic magnetization, $a = 1/\kappa = M_s/(3\chi^0)$.

However, when $(H+\alpha M)/a$ is made to converge to zero and α is not zero, then there must be M=0, but this is contrary to the experimental measurements shown in the graph of $M=M_r$ at H=0 (M_r is remanent magnetism). The single-value correspondence with the applied magnetic field is not established by the anhysteretic magnetization curve. Thus, the conventional anhysteretic magnetization equation is corrected as:

$$f(M') = M' - M_s \left[\coth\left(\frac{H + \alpha M'}{\alpha}\right) - \frac{a}{H + \alpha M'} \right] = 0$$
 (15)

Fig. 3 illustrates a comparison between the traditional and the modified anhysteretic magnetization curves. The analysis indicates that the magnetization properties of the





(b) Comparison of magnetization curves for $B_v=1.2T$

Fig. 3. (Color online) Comparison of anhysteretic magnetization curves.

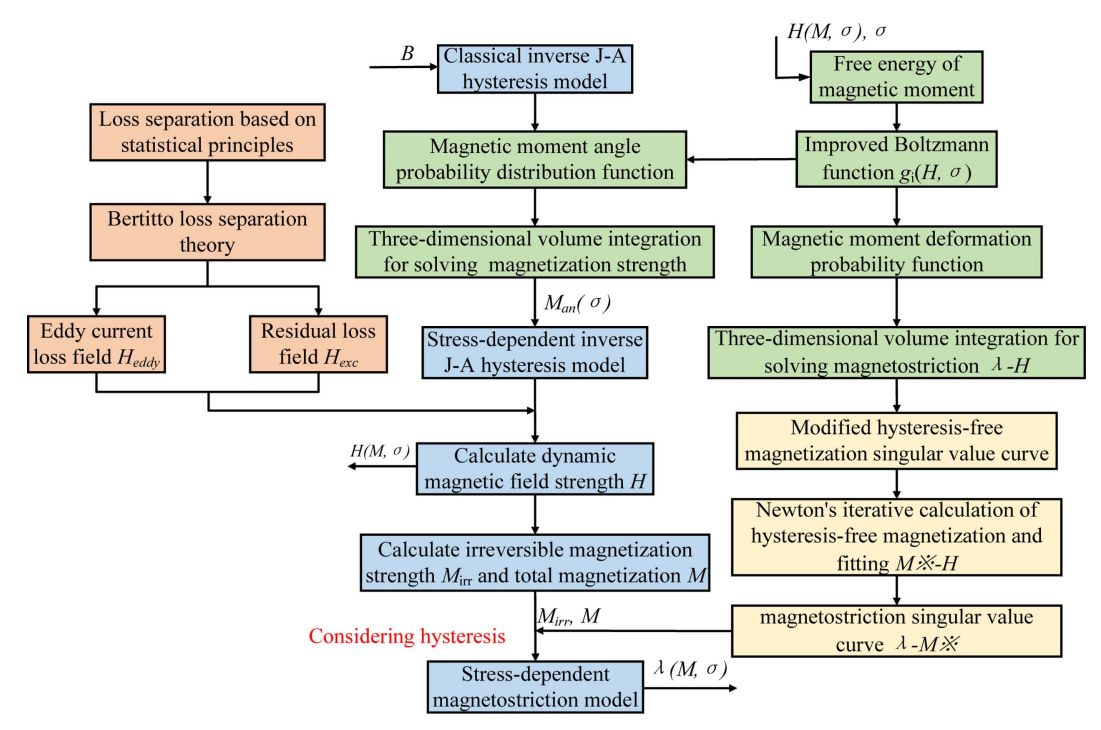


Fig. 4. (Color online) Simulation flow diagram of the magnetostriction model.

amorphous alloy are more precisely depicted by the modified magnetization curve.

The magnetic field strength H calculated from the dynamic inverse JA model was brought into the corrected anhysteretic magnetization equation. The anhysteretic magnetization strength M' was calculated by Newton's method [Eq. (16)] and the calculated M' and H were fitted, i.e., H = f(M').

$$\phi(M') = M' - \frac{f(M')}{f'(M')} \tag{16}$$

The results of the calculations in Eq. (16) are brought into Eq. (12):

$$\lambda = 2\lambda_s \left(\int_0^{2\pi} d\varphi \int_0^{\pi} g[f(M'), \sigma] \left| \cos \theta \right| \sin \theta d\theta - \frac{1}{2} \right) \tag{17}$$

From Eq. (17), the currently constructed magnetostriction model describes the single-value relationship between magnetostriction and magnetization strength. However, experimental measurements show that λ of amorphous alloys lags behind B (or M). The quantitative hysteresis behavior and irreversibility are mainly attributed to the irreversible magnetization strength of soft magnetic materials M_{irr} [13]. A comparison between the measured and the calculated results reveals that there is a slight variation in irreversible magnetostriction in the opposite direction to the applied magnetic field. Thus, this magnetostriction is corrected to:

$$\lambda = 2\lambda_s \left(\int_0^{2\pi} d\varphi \int_0^{\pi} g[f(\xi M + \eta M_{irr}), \sigma] \left| \cos \theta \right| \sin \theta d\theta - \frac{1}{2} \right)$$
 (18)

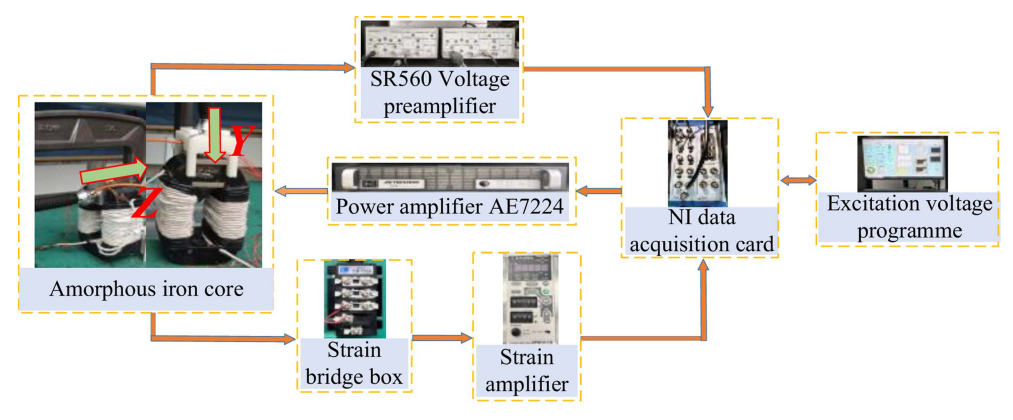
where η is a partial coefficient that varies with material type, ξ is a coefficient to be determined, and the parameters can be obtained through the process of fitting the experimental data.

Combining Eq. (5) to (18), the magnetostriction of amorphous alloys under compressive stresses in different directions can be simulated. A flowchart illustrating this process is presented in Fig. 4.

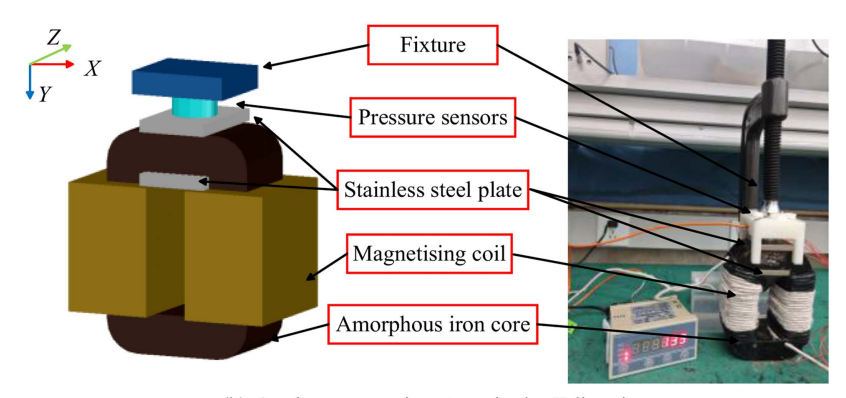
3. Magnetostriction Measurement of Amorphous Alloys

3.1. Experimental measurements and data analysis

To validate the correctness of the proposed magnetostriction model, a set of magnetic property measurement devices for measuring the magnetic properties and magnetostriction properties of amorphous alloys (grade 1K101, chemical composition: Fe:80%, Si+B:20%) is built in this paper. Due to the extreme thinness and fragility of the amorphous strip post-annealing, the amorphous core is engineered to be rolled from the amorphous alloy strip and subsequently annealed to alleviate internal stresses. The magnetic circuit apparatus comprises a series of excitation coils and induction coils, with the sample under examination measuring 135.04 mm in length, 91.07 mm in width, and 50.43 mm in thickness. The magnetic flux density waveform is controlled



(a) Magnetic properties system



(b) Apply compressive stress in the Y direction

Fig. 5. (Color online) Magnetostriction measurement.

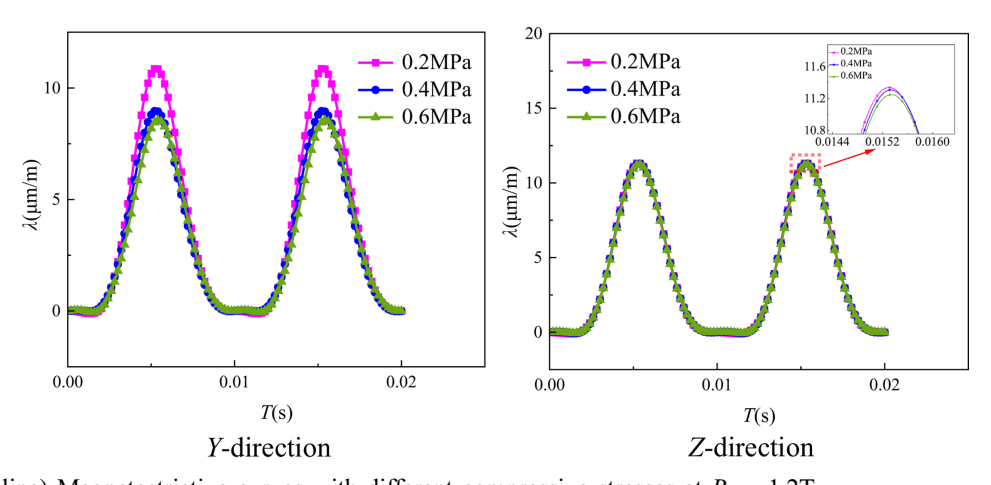


Fig. 6. (Color online) Magnetostrictive curves with different compressive stresses at $B_p = 1.2T$.

to be a standard sinusoidal signal with a frequency of 50 Hz by the constructed magnetic property measurement system, and its waveform coefficient is within $1.11 \pm 1\%$, which is in accordance with the international measurement standard of magnetic properties [14]. The measurement system utilized for the amorphous alloys is illustrated in Fig. 5(a). During the application of compressive stress to the amorphous core, a force is exerted on the C-type clamp

(which is non-conductive), allowing for the determination of compressive stress via a stress sensor, with the results displayed on a meter. The clamping device responsible for applying compressive stress in the Y direction is depicted in Fig. 5(b).

In the assessment of magnetostriction properties, the magnetostriction strain signal of an amorphous iron core is evaluated utilizing a resistive strain gauge. These resistance strain gauges are affixed to the surface of the core, ensuring that their horizontal orientation aligns with the direction of the magnetic circuit. The strain gauges are connected to a strain bridge box and a strain amplifier to facilitate the detection of strain signals. The resulting magnetostriction measurement curves over time, under varying directions of compressive stress, are illustrated in Fig. 6. The data indicate that the magnetostriction strain diminishes from 11.33946 to 11.24952 as the stress increases from 200 kPa to 600 kPa in the Z direction. Similarly, in the Y direction, the magnetostriction strain decreases from 10.88828 to 8.55974 with the same increase in stress.

3.2. Parameter extraction

The parameters required for the stress-dependent magnetostriction model established in this paper are extracted from the experimentally measured hysteresis loops and magnetostriction loops. The extraction method employed is the Velocity-Controlled Particle Swarm Optimization (VCPSO) algorithm [15]. In the optimization process, the parameters of the hysteresis model can be extrapolated to the parameters of the magnetostriction model. The flow chart of VCPSO parameter identification is shown in Fig. 7.

The hysteresis model parameters in this paper are determined by identifying hysteresis loops at the static saturation flux density B_p measured in the absence of stress, and the parameters are shown in Table 1. To extract the

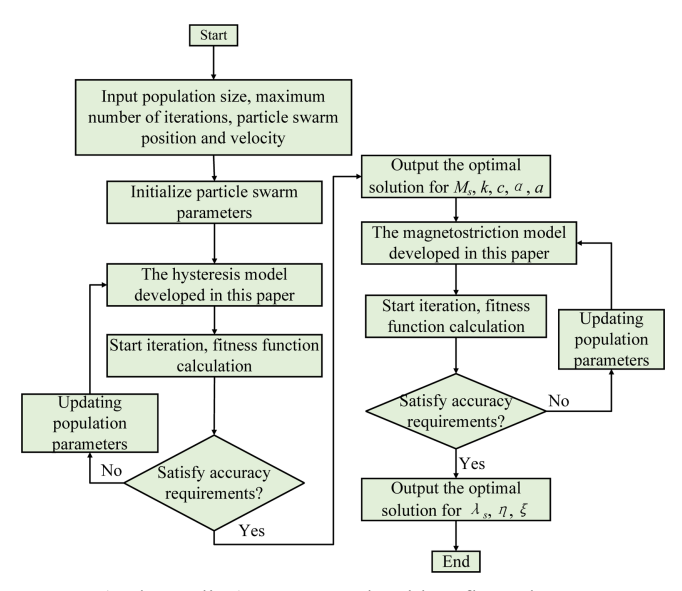


Fig. 7. (Color online) VCPSO Algorithm flow chart.

Table 1. Parameters of the hysteresis model.

$M_{\rm s}/({\rm A/m})$	k/(A/m)	a	α	c
1.40×10^{6}	184.499	458.99	9.712×10^{-4}	0.885

residual loss coefficient k_{exc} , the residual loss W_{exc} is first calculated from the hysteresis loops and total losses at f = 5 Hz and f = 50 Hz for different peak flux densities and stresses [14]. The expression for the residual loss under sinusoidal excitation is given by:

$$W_{exc} = 8.76k_{exc}B_n^{1.5}f^{0.5} (19)$$

According to the formula of residual loss under sinusoidal excitation, the residual loss coefficients k_{exc} under different peak flux densities B_p and stresses σ are identified, and a three-dimensional distribution surface plot illustrating dynamic parameter k_{exc} across different peak flux densities B_p and Y direction compressive stresses σ is constructed and presented in Fig. 8. The observation is that the residual loss coefficient k_{exc} increases with the rise in magnetic flux density at different stress conditions. The fitting equation of the residual loss coefficient k_{exc} to the flux density magnitude and stress is expressed as:

$$k_{exc} = 0.04695 + 0.12539\sigma + 0.14639B_{p} - 0.2086\sigma^{2} -0.02439B_{p}^{2} - 0.05416\sigma B_{p}$$
 (20)

Based on the expression obtained from the above fitting of the parametric nonlinear surface, the residual loss

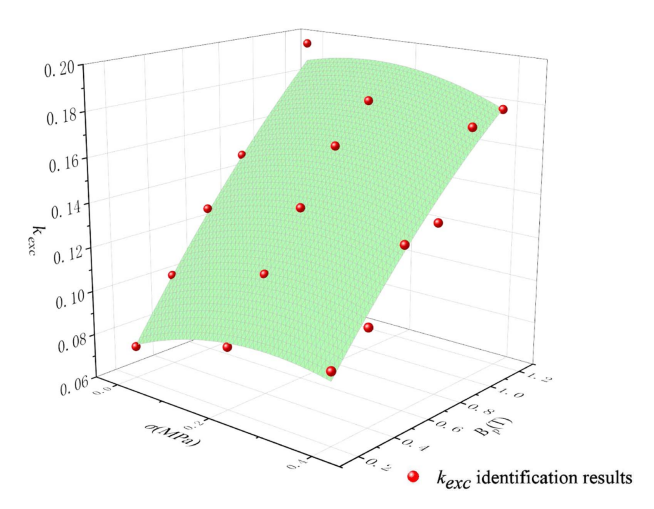


Fig. 8. (Color online) Residual loss coefficient k_{exc} 3D fitting plot.

Table 2. Magnetostriction parameters under different σ at 1.2T

	σ/MPa	ξ	η	$\lambda_{\rm s}/(\times 10^{-6})$
V 4:+:	0.2	0.152	0.988	64.865
Y-direction compressive stress	0.4	0.149	0.985	56.264
compressive suess	0.6	0.149	0.984	55.692
7. 1	0.2	0.158	0.986	66.472
Z-direction compressive stress	0.4	0.158	0.985	66.162
compressive suess	0.6	0.158	0.984	65.761

coefficient k_{exc} can be predicted for any flux density amplitude and stress. Then, employing the identified hysteresis model parameters as input, the magnetostriction model parameters are obtained according to the magnetostriction curves at different σ , as shown in Table 2.

4. Simulation Results and Discussion

Utilizing the derived model parameters in conjunction with the stress-related hysteresis model and the magnetostriction model presented in this study, simulations of the hysteresis and magnetostriction properties under varying orientations of compressive stresses at an excitation frequency of 50 Hz are conducted. These simulations are then compared with the corresponding experimental findings.

When compressive stresses of 200 kPa and 600 kPa are applied to the amorphous alloy core in the Y and Z directions, respectively, the outcomes derived from simulations of hysteresis loops and magnetostriction loops generally align with the experimental findings, as illustrated in Figs. 9 and 10. The application of compressive stress along the Z-direction does not significantly affect the magnetostriction of the amorphous alloy. In contrast, a marked change in magnetostriction is observed when compressive stress is applied in the Y-direction. A comparison of the magnetostriction loops at varying stress levels within the same direction reveals that the maximum magnetostriction

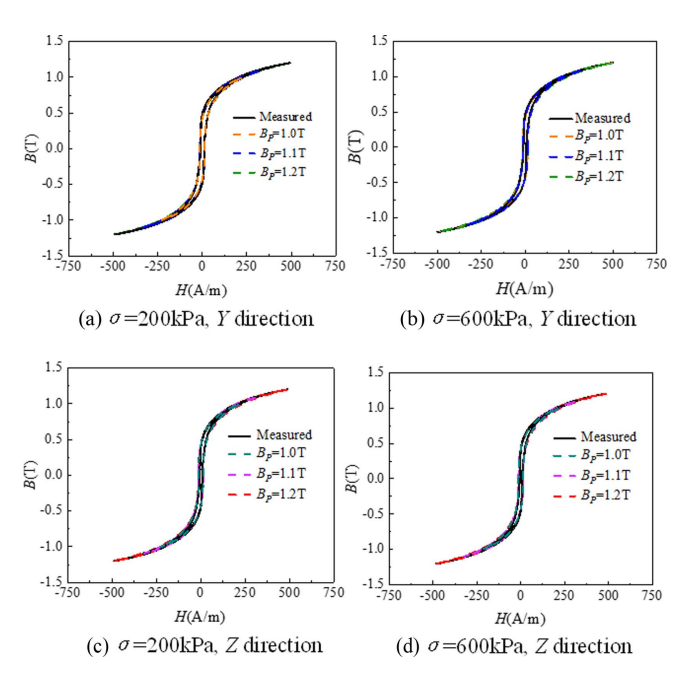


Fig. 9. (Color online) Comparison of simulated and measured hysteresis loops.

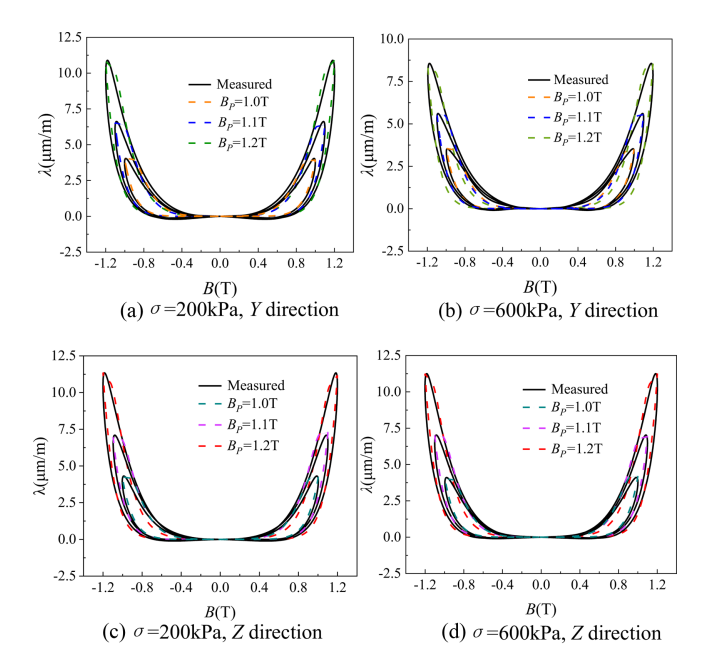


Fig. 10. (Color online) Comparison of simulated and measured magnetostriction loops.

strain of the amorphous alloys diminishes as compressive stress increases. This phenomenon indicates that the application of compressive stress modifies the movement and deflection of the magnetic moment within the amorphous alloy, thereby restricting the magnetic moment's ability to deflect in the direction associated with easy magnetostriction.

5. Conclusion

This study presents an enhanced micro-statistical model for amorphous alloys characterized by the absence of a crystalline structure and a random arrangement of atomic magnetic moments. By integrating this model with the inverse JA energy balance theory and the irreversible component, a refined stress-dependent magnetostriction model for amorphous alloys is developed, which takes into account the hysteresis effect. The proposed model effectively simulates the hysteresis loop and magnetostriction loop of amorphous alloys subjected to varying compressive stresses in multiple directions, thereby offering a robust framework for the precise prediction of vibrations in amorphous cores.

Acknowledgments

This work was supported by the National Natural Science Foundation of China under Grant No. 52477011, 52207012.

References

- [1] L. J. Li, S. H. Li, G. M. Li, D. R. Li, and Z. C. Lu, Mater. Res. Innov. **19**, S28 (2015).
- [2] P. Zhang and L. Li, Int. J. Electr. Power Energy Syst. 123, 106298 (2020).
- [3] Y. Li, Z. Yang, C. Zhang, C. Zhang, and S. Mu, IEEE Trans. Magn. **58**, 8401405 (2022).
- [4] A. A. Adly, I. D. Mayergoyz, and A. Bergqvist, J. Appl. Phys. 69, 5777 (1991).
- [5] T. Ben, F. Chen, L. Chen, and R. Yan, AIP Adv. 11, 015120 (2021).
- [6] H. Jiang, J. Zhu, and C. Yuan, J. Magn. Magn. Mater. 486, 165274 (2019).
- [7] L. Daniel, O. Hubert, N. Buiron, and R. Billardon, J. Mech. Phys. Solids 56, 1018 (2008).

- [8] L. Daniel, Eur. Phys. J. Appl. Phys. 83, 30904 (2018).
- [9] Y. Li, J. Zhu, Y. Li, H. Wang, and L. Zhu, J. Magn. Magn. Mater. 529, 167854 (2021).
- [10] L. Wu, K. Yao, B. Zhao, and Y.-S. Wang, Appl. Phys. Lett. 115, 162406 (2019).
- [11] A. P. S. Baghel and S. V. Kulkarni, IEEE Trans. Magn. 50, 7009004 (2014).
- [12] Y. Wang, L. Li, and X. Zhao, COMPEL. 42, 219 (2023).
- [13] Y. Li, J. Zhu, L. Zhu, Y. Li, and G. Lei, IEEE Trans. Magn. **56**, 7511405 (2020).
- [14] P. Fagan, B. Ducharne, S. Zurek, M. Domenjoud, A. Skarlatos, L. Daniel, and C. Reboud, IEEE Trans. Instrum. Meas. **71**, 6006113 (2022).
- [15] L. Chen, Q. Yi, T. Ben, L. Chen, X. Zhang, and Y. Kong, AIP Adv. 11, 015022 (2021).